UNCERTAINTY OF FULL-SCALE MANOEUVRING TRIAL RESULTS ESTIMATED USING A SIMULATION MODEL

Sergey Gavrilin*
NTNU Department of Marine Technology
7052, Otto Nielsens veg. 10, Trondheim, Norway
Email: sergey.gavrilin@ntnu.no

Sverre Steen
NTNU Department of Marine Technology
7052, Otto Nielsens veg. 10, Trondheim, Norway
Email: sverre.steen@ntnu.no

https://doi.org/10.1016/j.apor.2017.03.011

Highlights

- Result uncertainty due to environmental effects and other inputs is estimated.
- The analysis replaces costly repeated tests.
- Input uncertainties are propagated using Monte Carlo simulations.
- Variance decomposition shows contribution of the input factors.

Abstract

This paper describes how to estimate the uncertainty of manoeuvring sea trial results without performing repeated tests using only a simulation model. The approach is based on the Monte Carlo method of uncertainty propagation. Moreover, the global sensitivity analysis procedure based on variance decomposition is described. As an example, the method is applied to estimate the uncertainty of 10°/10° zigzag overshoot angles and a 20° turning circle advance and tactical diameter for a small research vessel. The estimated uncertainty is compared with corresponding experimental uncertainty assessed from repeated tests. The method can be useful for validation studies and other studies that involve the uncertainty of sea trial results.

Key words: uncertainty, Monte Carlo, sensitivity, manoeuvring

1 Introduction

Currently, ship manoeuvring simulation models are widely applied for training, standardization and engineering purposes. However, recent studies [1] have shown a large scatter in the results predicted by models developed by different organizations. This indicates high demand for the development of validation techniques, as well as for the improvement of ship simulation models. The ITTC Manoeuvring Committee indicates the importance and a lack of validation activities for ship simulators [2,3]. Validation is performed via comparison of predictions made by a simulator with experimental results for identical trials. Full-scale or model-scale experiments are used to obtain a benchmark for validation. However, model-scale experiments are prone to scale effects; therefore, full-scale experiments are preferable. Evaluation of the uncertainty of experimental results is an important part of validation. The ITTC issued a recommended procedure for the uncertainty analysis of free running model tests [4] that outlines the main sources of uncertainty in manoeuvring experiments. They use a combination of three approaches to obtain the combined uncertainty: measurement uncertainty analysis, repeatability analysis and uncertainty propagation analysis. The uncertainty propagation analysis is based on the Taylor series method. According to the method, the uncertainty of the experimental result due to some input factor is equal to the product of the uncertainty of this factor and the so-called uncertainty magnification factor (UMF). The UMF is a linear local absolute sensitivity coefficient and can be numerically estimated using a simulation model. The total combined uncertainty is calculated as the root summed squared of the individual uncertainty contributions. Although this approach can be partly applied to full-scale tests, some features cause a significant difference between full-scale tests and model-scale tests. The price of repetitions is very high for full-scale tests; therefore, the repetitions are rarely performed. Moreover, sea trial results are influenced by environmental effects, whose contribution to the resulting uncertainty is sometimes dominating. These effects are represented by two or more independent factors (such as current speed and direction, or wave height, period and direction) with strong interaction. Therefore, the combined result uncertainty cannot be estimated using the UMFs.

In this paper, we consider an alternative approach to uncertainty propagation based on the Monte Carlo method [5,6]. The Monte Carlo method is more flexible and suitable for highly nonlinear systems and interconnected input factors. The Monte Carlo method was previously used in manoeuvring to propagate the uncertainty of force measurements in captive tests to the final uncertainty of manoeuvring indices (overshoot angles) [7,8]. We apply the method to estimate the uncertainty of repeated tests and compare it with the experimentally determined uncertainty. We also describe the global sensitivity analysis based on variance decomposition and apply it to estimate the contribution of the input factors to the total uncertainty. Thus, the main goal of the paper is to demonstrate how to estimate uncertainty of full-scale manoeuvring tests in practice, without actually performing repeated tests. Therefore, we do not consider some possible sources of uncertainty which are negligible, while focusing on more important ones. We emphasize also that all the sensitivity coefficients obtained are specific for the case vessel and prescribed conditions. However, the same algorithm can be applied to any other vessel.

The paper is organized as follows. Section 2 describes the Monte Carlo method of uncertainty propagation. Section 3 describes how to estimate the contribution of the input factors to the total uncertainty of the result using graphical analysis and variance decomposition. Section 4 describes how to use the Monte Carlo method to estimate the uncertainty of manoeuvring trial results. Section 5 presents an example of the application of the analysis to estimate the uncertainty of 10°/10° zigzag and 20° turning circle test results. Section 6 contains discussion and conclusions.

2 Monte Carlo method

Consider the result Y predicted by a simulation model. The result depends on the set of uncertain input factors $\boldsymbol{X}$:

$$Y = f\left(\boldsymbol{X}\right) \tag{1}$$

Each of the input factors in $\boldsymbol{X}$ has an associated known probability distribution. The goal of the Monte Carlo propagation method is to estimate the uncertainty of Y due to the uncertainty of $\boldsymbol{X}$. The following algorithm describes the procedure:

1. Generate a matrix $\boldsymbol{A}$ with numbers distributed randomly on [0, 1], with N rows and k columns, where N is a sufficiently large number, k is the number of input factors in $\boldsymbol{X}$. N defines the total number of simulations.
2. Apply the corresponding inverse cumulative distribution function to the samples of each column and compose a new matrix $\boldsymbol{X}$ from the resulting numbers:

$$x_{ji} = CDF_i^{-1}\left(a_{ji}\right) \tag{2}$$

3. Now, each row of the matrix $\boldsymbol{X}$ contains a set of input parameters for (1). Perform the simulations for each row of $\boldsymbol{X}$ and calculate the array of results $\boldsymbol{Y}$ according to (1).
4. According to the central limit theorem [9], the result $\boldsymbol{Y}$ is distributed approximately normally if it is not dominated by a single input factor. Therefore, calculate the standard deviation σ of $\boldsymbol{Y}$ and then calculate expanded uncertainty U_{95} by multiplying σ by the coverage factor 2. In some cases, the resulting distribution of $\boldsymbol{Y}$ is not close to a normal distribution. Then, to find the 95% confidence interval, build the empirical CDF of $\boldsymbol{Y}$ and find the lower and the upper border of the confidence interval as the argument of the function, where it equals 0.025 and 0.975, respectively.

Thus, the Monte Carlo method provides the uncertainty of the model output due to the uncertainty of the input factors $\boldsymbol{X}$. However, the method does not provide information regarding the contribution of each individual input factor to the total uncertainty.

3 Global sensitivity analysis

In the Taylor series method of uncertainty propagation, the individual contributions of the input factors' uncertainty are calculated as a part of the analysis. In the Monte Carlo method, it is not possible to say directly which input parameters make the main contribution to result uncertainty. However, this knowledge is very useful. It increases confidence in the uncertainty analysis and helps to detect faults or to improve the experiment.

We consider two methods to assess the relative importance of the input factors. The first method is graphical. According to the method, one should plot the result Y versus the input factor X_i (this will be illustrated in subsection 5.5, see Figure 6). If the result changes for different values of the input factor, or, in other words, a pattern is observed, the parameter is important. The stronger the pattern is, the more important the parameter is. The method is simple and does not demand additional simulations. However, it does not give any objective quantitative measure of the factor's importance, and it is not suitable for studying the joint effects of several interacting factors.

The second method is based on variance decomposition. The further description of the method closely follows [10,11]. The method uses the concept of a sensitivity index as the measure of factors' importance. There are first-order, joint and total effect sensitivity indices. The first-order sensitivity index S_i and the total effect S_{Ti} of the factor X_i are defined correspondingly as:

$$S_i = \frac{V_{X_i}\left(E_{\boldsymbol{X}_{\sim i}}(Y \mid X_i)\right)}{V(Y)} \tag{3}$$

$$S_{Ti} = \frac{E_{\boldsymbol{X}_{\sim i}}\left(V_{X_i}(Y \mid \boldsymbol{X}_{\sim i})\right)}{V(Y)} = 1 - \frac{V_{\boldsymbol{X}_{\sim i}}\left(E_{X_i}(Y \mid \boldsymbol{X}_{\sim i})\right)}{V(Y)} \tag{4}$$

where $V_{Xi}(...)$, $E_{Xi}(...)$ is the variance and the mean, respectively, of the argument *(...)* taken over X_i; $V_{\boldsymbol{X}\sim i}(...)$, $E_{\boldsymbol{X}\sim i}(...)$ is the variance or mean of the argument *(...)* taken over all factors but X_i; *V(Y)* is unconditional variance. Thus, S_i is the expected relative reduction in variance *V(Y)* that would be obtained if X_i could be fixed; S_{Ti} is the expected relative variance that would be left if all factors but X_i could be fixed. The joint sensitivity indices are defined by analogy, for instance, for two factors:

$$S_{i,j}^{c} = \frac{V_{\boldsymbol{X}_{ij}}\left(E_{\boldsymbol{X}_{\sim ij}}\left(Y \mid \boldsymbol{X}_{ij}\right)\right)}{V\left(Y\right)} \tag{5}$$

The higher-order effects (interactions) are defined as the residual component as:

$$S_{ij} = S_{i,j}^{c} - S_i - S_j \tag{6}$$

In fact, the unconditional variance can be decomposed as the sum of the first-order and higher-order effects:

$$1 = \frac{V\left(Y\right)}{V\left(Y\right)} = \sum_i S_i + \sum_i \sum_{j>i} S_{ij} + \sum_i \sum_{j>i} \sum_{l>j} S_{ijl} + \ldots + S_{12\ldots k} \tag{7}$$

The total effect of the factor X_i contains all terms in (7) that involve this factor, for instance:

$$S_{T1} = S_1 + S_{12} + S_{13} + S_{123} + \ldots \tag{8}$$

To sum up the method, we list important properties of the sensitivity indices:

- S_i and S_{Ti} are numbers between 0 and 1. Higher value indicates higher influence.
- $S_{Ti} = 0$ means that X_i does not influence Y and can be fixed.
- S_i shows the primary effect of the factor X_i. The difference $(S_{Ti} - S_i)$ is the measure of the interaction between X_i and the other input factors. $S_{Ti} = S_i$ indicates the absence of the interaction.

One can use the following algorithm to estimate S_i and S_{Ti} numerically:

1. Generate a $2k$-dimensional Sobol sequence of quasi random numbers of length N (k – number of input parameters, N – sufficiently large number). The function '*sobolset*' can be used in Matlab. Split the sequence into two matrices: $\boldsymbol{A}$, containing first k columns of the sequence, and $\boldsymbol{B}$, containing the remaining k columns.
2. Compose auxiliary matrices $\boldsymbol{A}_{\boldsymbol{B}}^{(i)}$, where all columns come from $\boldsymbol{A}$ except for the i^{th} column, which comes from $\boldsymbol{B}$.
3. For each column, use the mapping function CDF_i^{-1} that maps, uniformly distributed on [0, 1], numbers to the custom distributions according to (2). For simplicity, we keep the notation of the matrices.
4. Run simulations using each row from the matrices $\boldsymbol{A}$, $\boldsymbol{B}$ and $\boldsymbol{A}_{\boldsymbol{B}}^{(i)}$ as the input of model (1) and calculate corresponding outputs $f(\boldsymbol{A})$, $f(\boldsymbol{B})$ and $f(\boldsymbol{A}_{\boldsymbol{B}}^{(i)})$.
5. Calculate variance *V(Y)* using $f(\boldsymbol{A})$ and $f(\boldsymbol{B})$.
6. Estimate conditional variances and expectations using formulas:

$$V_{X_i}\left(E_{\boldsymbol{X}_{\sim i}}\left(Y|X_i\right)\right) = V\left(Y\right) - \frac{1}{2N}\sum_{j=1}^{N}\left(f\left(\boldsymbol{B}\right)_j - f\left(\boldsymbol{A}_{\boldsymbol{B}}^{(i)}\right)_j\right)^2 \tag{9}$$

$$E_{\boldsymbol{X}_{\sim i}}\left(V_{X_i}\left(Y|\boldsymbol{X}_{\sim i}\right)\right) = \frac{1}{2N}\sum_{j=1}^{N}\left(f\left(\boldsymbol{A}\right)_j - f\left(\boldsymbol{A}_{\boldsymbol{B}}^{(i)}\right)_j\right)^2 \tag{10}$$

7. Calculate S_i using (3) and (9) and S_{Ti} using (4) and (10).

Instead of the Sobol sequence, one can use random numbers to compose the design matrices ***A*** and ***B***. However, more simulations can be necessary to achieve convergence. For alternative sampling techniques and formulas for conditional variance and mean, consult [10]. One needs *N(k+2)* simulations to estimate S_i and S_{Ti} for each input factor. The uncertainty of the result is obtained as part of the analysis (in step 5); therefore, no separate Monte Carlo simulations are needed. To calculate sensitivity indices for the joint effects, one needs to compose additional auxiliary matrices in step 2, substituting several columns instead of one column from ***B***.

The analysis based on variance decomposition is more objective compared to the graphical analysis. It provides the quantitative measures of the relative importance of the input factors and allows for investigating interaction effects. However, it demands more simulations than one needs for the Monte Carlo analysis itself.

4 Application to manoeuvring trial results

It is very expensive (and sometimes impossible) to perform multiple repetitions of the trial to estimate uncertainty statistically. Instead, the simulation model can be used. Thus, the Monte Carlo simulations represent virtual experiments with varying input factors. System-based manoeuvring models typically allow accounting for: uncertainties in control parameters, such as rudder angles, rpm and execute time; kinematic parameters during approach and initial conditions; current speed and direction; wind speed and direction; wave parameters (for combined manoeuvring and seakeeping models); mass and moments of inertia; measurement uncertainty. The distributions for the factors should be based on the observations during the experiment and the problem statement (an example is given below). Sometimes, a single physical parameter can have multiple associated uncertainties, which are considered as separate input factors with their own probability distributions. For instance, rudder angle can have associated bias uncertainty (non-zero neutral rudder angle) and random uncertainty (deviation from the commanded value, changing each rudder execution). Important factors that cannot be included in the Monte Carlo analysis are loading conditions and the corresponding change of hydrodynamic effects (this would demand recalculation of all hull hydrodynamic coefficients at each iteration of Monte Carlo simulations). These factors are not revealed in repeated tests (unless the loading conditions change). However, they are important for validation analysis. Uncertainty due to loading conditions can be estimated using CFD or another numerical method, and the Taylor series method of uncertainty propagation can be applied as explained in [4]. Thus, the total combined uncertainty of the result is calculated as:

$$u_C(Y) = \sqrt{\left(u_{C_{Meas}}(Y)\right)^2 + \left(u_{C_{MCM\ prop}}(Y)\right)^2 + \left(u_{C_{TSM\ prop}}(Y)\right)^2} \tag{11}$$

where $u_{C\_Meas}(Y)$ is the measurement uncertainty of Y, $u_{C\_MCM\_prop}(Y)$ is the propagation uncertainty for the factors that can be varied at each simulation and are estimated using the Monte Carlo method, and $u_{C\_TSM\_prop}(Y)$ is the propagation uncertainty for the factors that cannot be varied at each simulation and are estimated using the Taylor series method.

5 Case study: uncertainty of repeated tests

5.1 Case vessel description

In this study, we use a relatively small (31.25 m overall length) research vessel, i.e., “Gunnerus”, as a case vessel (Figure 1). The ship is owned and operated by the Norwegian University of Science and Technology (NTNU), which makes it cheaper and easier to access for full-scale trials for research purposes. Due to this fact, it is possible to perform repeated tests. Table 1 lists the main parameters of the vessel. “Gunnerus” is equipped with two ducted propellers and two flapped rudders. The diesel-

electric propulsion system comprises main electric propulsion (2 x 500 kW) and the bow tunnel thruster (200 kW), powered by generators (3 x 500 kW). The cruising speed of the vessel is 10.5 knots.

Figure 1. Research vessel "Gunnerus".

Table 1. Main dimensions of research vessel "Gunnerus".

Length overall [m]	31.25
Length between perp. [m]	28.90
Length in waterline [m]	29.90
Breadth midships [m]	9.60
Mast height / antenna [m]	14.85 / 19.70
Dead weight [t]	107

5.2 Measurement equipment

To register ship motions, two integrated orientation and position sensors produced by Kongsberg Seatex were used: the permanently mounted Seapath 330+ with correction signals and the temporarily installed Seapath 330. The sensors combine GNSS signals and inertial measurements. Table 2 demonstrates some accuracy limits of the measurement system. Further information can be found on the webpage of the supplier (http://www.km.kongsberg.com).

Table 2. Accuracy of the Seapath 330+ measurements, i.e., RMS, according to the manufacturer (position depends on the distance to the closest correction station).

Heading	0.04°
Position (X and Y)	1 cm + 1 ppm
Velocity	0.03 m/s

Propeller RPMs were measured via optical measurement of pulses from the shaft. Wire-over-potentiometer distance sensors attached to each rudder stock were used for rudder angle measurements. The sensors were calibrated using the mechanical indicators on top of the rudder stocks. Rudder measurements by the DP system of the vessel were also recorded, where available. Wind direction and speed were measured by the wind sensor mounted on the mast of the ship, approximately 10 m above the water surface.

Apart from the measurement equipment on the ship, two wave buoys were used. An advanced Fugro Oceanor Wavescan buoy was anchored near the trial site during the first series of trials (further referred to as "the fjord trials"). The buoy measures the directional wave spectrum, current speed and direction at 1.5 m depth, wind speed and direction, and some other parameters. For the second series of trials (further referred to as "the ocean trials"), a drifting Datawell DWR-G4 40 cm buoy was used. The buoy measures only its own position and a directional wave spectrum.

5.3 Experimental program and conditions

Results from two different series of trials are used in the paper. Both were performed near Trondheim, Norway. The first series of trials (the fjord trials) was conducted in August 2013 in the Trondheim fjord (N 63° 29.717', E 10° 27.951'). The program included 10°/10° and 20°/20° zigzag tests with different approach speeds, executed both manually and in the automatic mode, 20° and 35° turning circles, speed tests, and some low speed and DP tests. In the automatic mode, the rudder is controlled by a special program in the DP system, which is made to automatically execute 10°/10° and 20°/20° zigzag tests. The fjord area is well sheltered, so despite the relatively strong wind (sometimes up to 8-10 m/s), the significant wave height was typically 0.2 – 0.3 m. Current speed measured by the buoy was up to 0.4 m/s; the direction of the current varied due to tides and two rivers flowing into the fjord. The second series (the ocean trials) was conducted in the open ocean (N 63° 35.334', E 8° 5.980') in November 2013, with an emphasis on turning circles. Several tests were executed in a sheltered area behind islands, where no significant waves were observed. Wind speed was up to 6 m/s. Current was estimated by applying the IMO correction procedure [12] for each turning manoeuvre:

$$\bar{\boldsymbol{V}}_C = \frac{1}{N}\sum_{i=1}^{N}\frac{\boldsymbol{r}(\psi_i + 2\pi) - \boldsymbol{r}(\psi_i)}{t(\psi_i + 2\pi) - t(\psi_i)} \tag{12}$$

where points ψ_i are chosen during steady turning, then equal points $\psi_i+2\pi$ are found on the next turn, and then corresponding differences of position $\boldsymbol{r}$ and time t are calculated. Note that in general, this estimate includes the actions of other factors, such as wind and waves. Current speed estimated using (12) was up to 0.5 m/s.

5.4 Results of trials

For demonstration, we focus only on two types of trials: 10°/10° zigzag (1st overshoot and 2nd overshoot angles) and 20° turning circle (advance and tactical diameter). The trials are executed in automatic mode. Five repetitions of each trial are used. Table 3 contains the mean values of first and second overshoot angles from the zigzag tests, standard uncertainty and relative expanded uncertainty, with 95% confidence. The latter one is calculated using a coverage factor of 2.776, taken from two tail Student's t-distribution, with 95% confidence for four degrees of freedom (equal to the number of experiments minus one). Figure 2 demonstrates the time series of the heading and both rudder angles for the zigzag tests. It is easy to see some reasons for the scatter of overshoot angles. The rudder angles differ from the commanded 10° or –10° (the deviations are within 1°). The 2nd and 3rd rudder executions occur with some delay after variation of the heading reaches 10° (the mean of the delays is 1.6° and 2.1°, with a standard uncertainty of 0.3° and 0.5° for the 2nd and 3rd rudder executions, correspondingly). The rudders deviate 1°–2° during approach to keep the vessel on a straight course (which also causes deviations of yaw rate during the 1st execution).

Table 3. Results of 10°/10° zigzag tests.

	1st OA	2nd OA
mean [deg]	8.5	7.9
σ [deg]	0.5	0.4
U_{95} [%]	16.7	13.9

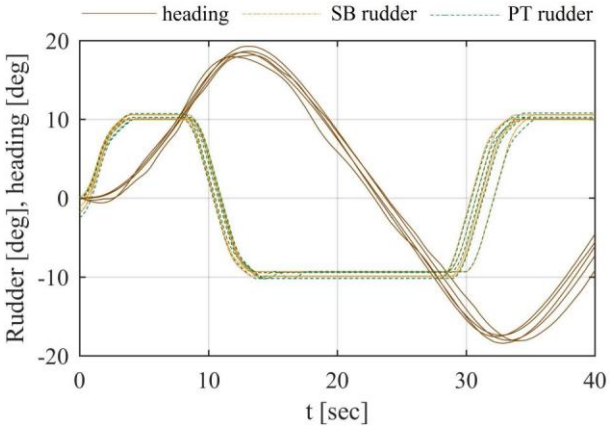

Figure 2. Results of 10°/10° zigzag trials.

Table 4 contains the mean values of advance and tactical diameter from the turning circle tests. Corrected values after applying (12) are also included.

Table 4. Results of the turning circle tests

	Advance		Tactical diam.	
	not cor.	cor.	not cor.	cor.
mean [m]	92.8	91.0	118.0	115.3
σ [m]	7.2	1.5	7.7	1.4
U_{95} [%]	21.7	4.5	18.2	3.4

5.5 Uncertainty and sensitivity analysis

In this section, we demonstrate how to estimate the uncertainty of repeated tests using a simulation model. The model is described in the Appendix. For simplicity, we neglect the measurement uncertainty, as it is negligible compared to uncertainty due to environmental effects and control factors. We also neglect all bias sources of uncertainty as they do not change during the tests series. Thus, the analysis answers the question "what would the uncertainty be if the test was repeated multiple times under particular conditions". These conditions are based on the observations made during the sea trials.

Table 5 lists input factors that are treated as uncertain in simulations of the turning circle test, with corresponding PDFs. All other model parameters are fixed and therefore do not affect the random uncertainty of the result. As no adjustment with respect to wind and current directions was made during the trials, every direction is equally possible. The uncertainty of initial conditions is presented by a single factor – the initial rudder deviations. The total number of simulations performed is 4000. Figure 3 and 4 demonstrate distributions of the values of advance and tactical diameter for a corrected turning circle resulting from the Monte Carlo simulations. Table 6 presents the mean values, standard deviations and expanded uncertainty (a coverage factor of 2 is used) of advance and tactical diameter both for corrected and non-corrected turning circles. From the comparison of Table 4 and Table 6, it follows that the Monte Carlo analysis gives reasonable estimates of the uncertainties, although for the advance, the value of uncertainty is lower in the simulations. The mean values are also similar.

Table 5. Input factors with distributions for turning circle simulations.

ID	Input factor	Distribution
1	Wind direction [deg]	U(0, 360)
2	Wind speed [m/s]	N(5, 2)
3	Current direction [deg]	U(0, 360)
4	Current speed [m/s]	N(0.25, 0.07)
5	Initial rudder dev. [deg]	U(-1, 1)
6	SB rudder dev. [deg]	U(-0.5, 0.5)
7	PT rudder dev. [deg]	U(-0.5, 0.5)

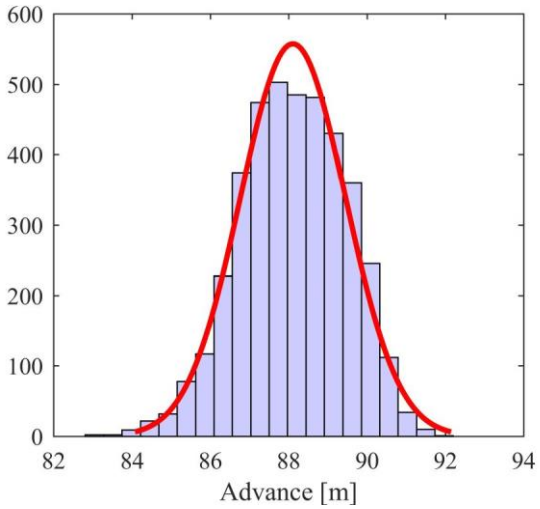

Figure 3. Results of Monte Carlo simulations of turning circles with correction: advance.

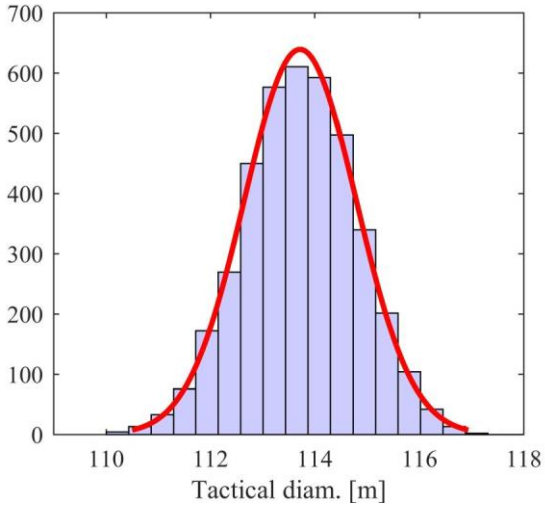

Figure 4. Results of Monte Carlo simulations of turning circles with correction: tactical diameter.

Table 6. Results of Monte Carlo simulations of turning circles.

	Advance	Advance (corr)	Tact. diam.	Tact. diam. (corr)
mean [deg]	88.1	88.1	113.7	113.7
σ [deg]	4.7	1.3	8.6	1.1
U_{95} [%]	10.7	3.1	15.2	1.9

To identify which of the factors from Table 5 make the largest contribution to the uncertainty of the results, we perform a sensitivity analysis. Figure 5 demonstrates the first-order sensitivity indices and the total effects for advance. For the current direction and current speed, the total effect is higher than the first-order sensitivity index. The same holds for the wind direction and speed, although less obviously. This difference indicates the presence of interaction between the input factors. The alternative way to see whether the input factor is important is graphical analysis. Figure 6 demonstrates advance resulting from Monte Carlo simulations plotted versus some input factors. A strong effect is observed for the current direction. There is also some pattern for current speed. However, the mean values of advance for each current speed are approximately the same. Therefore, there is strong interaction of current speed with other factors. A weaker effect is observed for wind direction, while almost no effect is observed for rudder deviation. Thus, graphical analysis leads to the same conclusions as variance-based analysis.

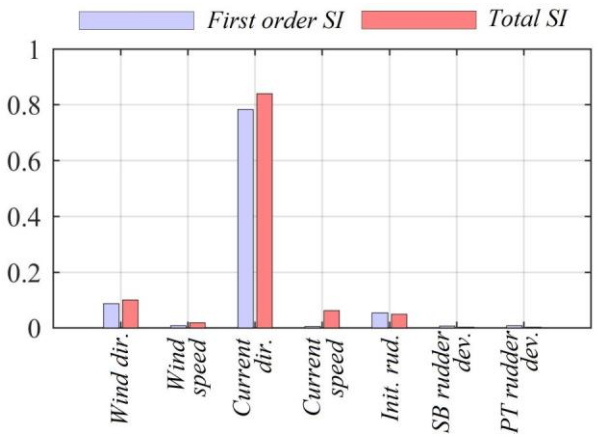

Figure 5. Sensitivity indices for advance (without correction).

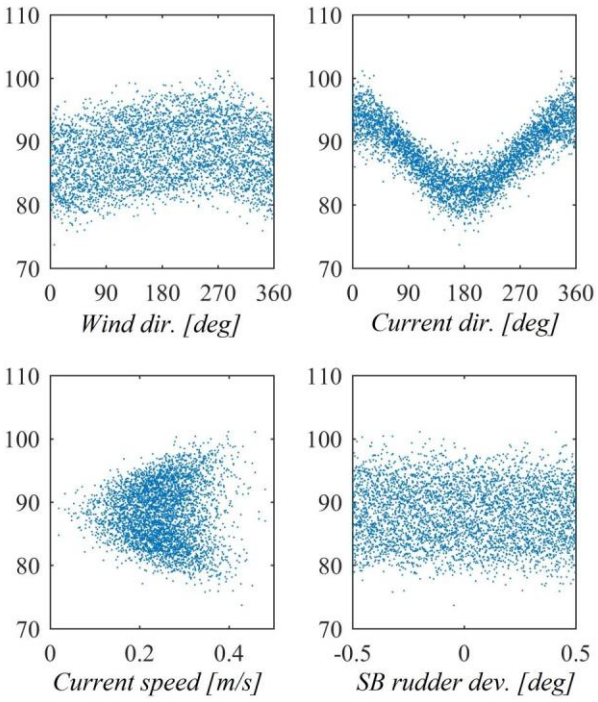

Figure 6. Advance [m] vs input parameters.

Figure 7 and 8 present the sensitivity indices of the advance and the tactical diameter for non-corrected and corrected turning circles, where related input factors are combined. In both cases, the current effect is the main contribution to the combined uncertainty of the results for the non-corrected trajectory. The other factors are much less important. However, the effect of current is negligible if the correction is applied. The effect of wind is also partly reduced. Nevertheless, it becomes an important contribution to the total uncertainty of both results. A significant part of the total uncertainty of advance after correction is due to uncertainty in the initial conditions. The rudder deviation from the commanded value gives the main contribution to the advance for the corrected turning circle. These results are reasonable: initial conditions affect time when the heading changes by 90° or 180° and therefore have high influence on the distance travelled along the approach direction (but not in the transverse direction), while small rudder deviations affect the curvature of the track.

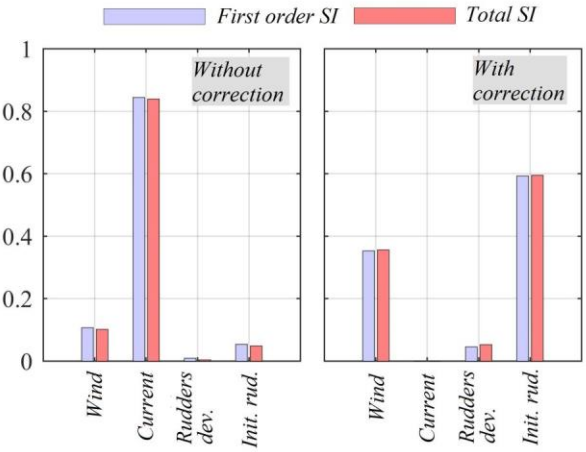

Figure 7. Sensitivity indices for the advance (without and with correction).

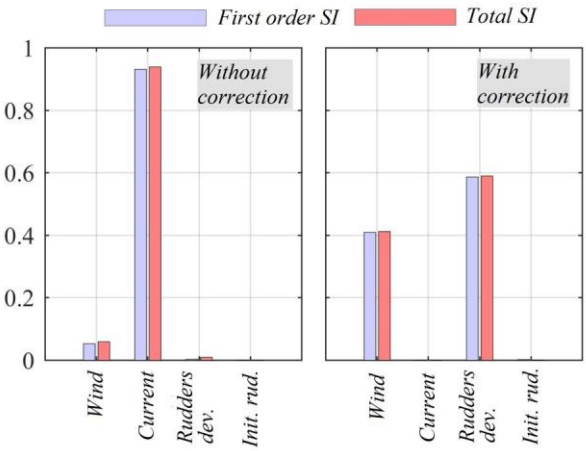

Figure 8. Sensitivity indices for the tactical diameter (without and with correction).

Table 7 lists input factors that are treated as uncertain in the simulations of zigzag tests. The initial rudder deviation accounts for uncertainty in the initial conditions during the first execution. The heading deviations during the 2nd and 3rd execution account for the delay in the DP system controlling the automatically executed zigzag trials. Because the ship is small and responds quickly, the 2- to 4-second delay from detecting the threshold heading change to executing the rudder was a major problem, which was only partly compensated for by means of trial and error lowering of the actuation threshold angle from 10° or 20° to lower angles. In fact, the mean value of the heading that activates the rudder execution in the simulations is 12° instead of 10° to increase the similarity of the simulations to the experiment. Rudder deviations from commanded values are independent for each rudder and each execution. The effect of the current is not included as it does not affect the heading.

Table 7. Input factors with distributions for zigzag simulations.

ID	Input factor	Distribution
1	Wind direction [deg]	N(0, 15)
2	Wind speed [m/s]	N(5, 2)
3	Initial rudder dev. [deg]	U(-1, 1)
4	Heading dev. 2nd exec. [deg]	N(0, 0.5)
5	Heading dev. 3rd exec. [deg]	N(0, 0.5)
6	SB rudder dev. 1st exec. [deg]	U(-0.5, 0.5)
7	PT rudder dev. 1st exec. [deg]	U(-0.5, 0.5)
8	SB rudder dev. 2nd exec. [deg]	U(-0.5, 0.5)
9	PT rudder dev. 2nd exec. [deg]	U(-0.5, 0.5)
10	SB rudder dev. 3rd exec. [deg]	U(-0.5, 0.5)
11	PT rudder dev. 3rd exec. [deg]	U(-0.5, 0.5)

Figure 9 and 10 demonstrate the histogram of the first and second overshoot angles resulting from Monte Carlo simulations of the zigzag test and corresponding normal distributions. The total number of simulations is 4000. Table 8 contains the mean values, the standard deviations and the relative expanded

uncertainties of the overshoot angles. For the expanded uncertainties, a coverage factor of 2 is used. Comparing Table 3 and Table 8, we see that both the mean values and the expanded uncertainties are similar.

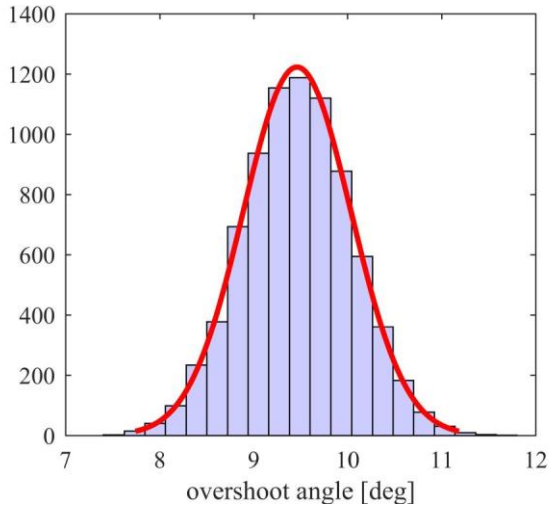

Figure 9. Results of Monte Carlo simulations of the zigzag trial: 1st overshoot angle.

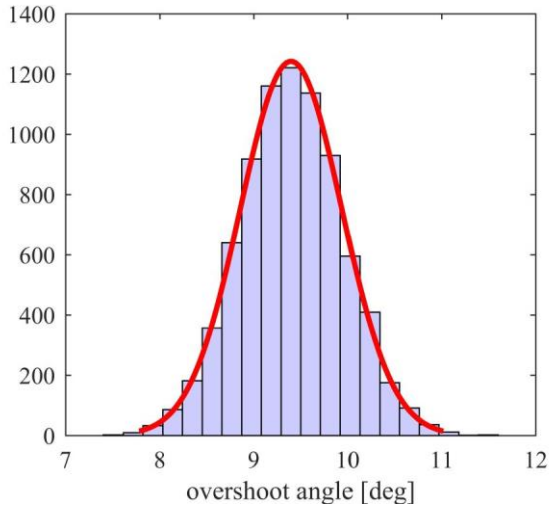

Figure 10. Results of Monte Carlo simulations of the zigzag trial: 2nd overshoot angle.

Table 8 Results of Monte Carlo simulations of the zigzag test

	1st OA	2nd OA
mean [deg]	9.5	9.4
σ [deg]	0.6	0.6
U_{95} [%]	12.5	12.1

To evaluate the contribution of each of the factors to the total uncertainty of the result, we perform global sensitivity analysis. Figure 11 presents the sensitivity indices. For convenience, we grouped related factors such as wind speed and direction and starboard and port rudder deviations for the same execution. We now see that the uncertainty of the heading at the time of change of the rudders preceding the corresponding overshoot angle is the largest contribution to the total uncertainty. The rudder deviation (previously the overshoot) and wind also have some influence. The rest of the input factors are insignificant. The importance of the heading deviation is easy to understand: if heading during the rudder

execution is different from the "planned" value (for example, 11° instead of 10°), this difference will directly affect the result (that is, that 1° will be added to the corresponding overshoot angle).

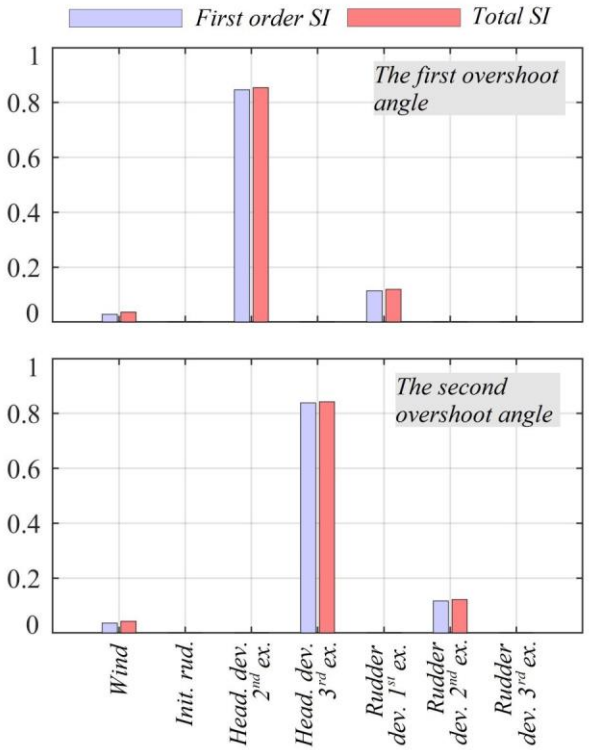

Figure 11. Sensitivity indices for the first (top) and second (bottom) overshoot angles.

6 Discussion and conclusions

In the paper, we have demonstrated how to estimate the uncertainty of the results of manoeuvring trials due to environmental effects and other factors without performing repeated tests. Although not all factors affecting the results can be included in the analysis, the approach may give a reasonable estimate of the uncertainty of the result and significantly reduce the cost of analysis. Contrary to the Taylor series propagation method, the Monte Carlo method considered in the paper is suitable for the cases when the relation between a result and input factors is nonlinear and interaction effects between different input factors are important. It is easy to apply the method and interpret the results. However, the method demands multiple simulations; thus, it is applicable to system-based models with input factors that can easily be varied. The choice of the distributions of the input factors is very important for the estimated uncertainty of the result. Therefore, one should make this choice with care, for instance, based on observations during the sea trials. However, we would like to emphasise that it is much easier to make good engineering estimates of the uncertainty of input variables such as wind and current than to directly estimate the uncertainty of the output results trials. This is actually the key contribution of this paper.

We have also demonstrated how to assess the contribution of individual input factors to the total uncertainty. The graphical method does not demand additional simulations. However, only the global sensitivity analysis based on the variance decomposition provides quantitative measures of the importance of the different factors and shows joint effects. Performing the global sensitivity analysis reduces the risk of a fault in the uncertainty analysis. The uncertainty estimates and the sensitivity of factors hold only for a specific vessel and specific input parameters. For instance, if the same simulations were performed with random wind direction, the combined uncertainty of overshoot angles and the sensitivity to wind would be bigger. Similarly, the delays of reaction and actuation of the control system or helmsman are important for this vessel, as it has a particularly fast reaction; however, they are mostly insignificant for slow reacting vessels. The analysis may be useful both in the design stage of the

experiment to assess the possible uncertainty of the results and importance of different factors and possibly modify the experiment to reduce the uncertainty of the result and after the experiment to estimate the actual uncertainty.

Acknowledgements

The research, as a part of the SimVal project, is sponsored by the Norwegian Research Council (225141/O70); the support is greatly acknowledged by the authors. We would also like to express our gratitude to MARINTEK for technical and professional help, as well as to the captain and crew of R/V "Gunnerus" for their great patience and good seamanship during the trials.

Nomenclature

σ	Standard deviation
CDF	Cumulative distribution function
$N(\mu, \sigma)$	Normal distribution with the mean μ and the standard deviation σ
OA	Overshoot angle
PDF	Probability distribution function
$U(\xi_1, \xi_2)$	Uniform distribution, with the lower and upper borders ξ_1 and ξ_2
U_{95}	Expanded uncertainty, with 95% confidence
UMF	Uncertainty magnification factor

References

[1] Stern F, Agdrup K, Kim SY, Hochbaum AC, Rhee KP, Quadvlieg F, Perdon P, Hino T, Broglia R, Gorski J. Experience from SIMMAN 2008-The First Workshop on Verification and Validation of Ship Maneuvering Simulation Methods. J Sh Res 2011;55:135–47.

[2] ITTC. Manoeuvring Committee Final Report and Recommendations to the 26th ITTC. vol. I. 2011.

[3] ITTC. Manoeuvring Committee Final Report and Recommendations to the 27th ITTC. 2014.

[4] ITTC. ITTC Uncertainty Analysis for Free Running Model Tests 7.5-02-06-05 2014.

[5] Coleman HW, Steele WG. Experimentation, Validation, and Uncertainty Analysis for Engineers. 3rd edition. Hoboken, NJ, USA: John Wiley & Sons, Inc.; 2009. doi:10.1002/9780470485682.

[6] Joint Committee for Guides in Metrology. Evaluation of measurement data — Supplement 1 to the "Guide to the expression of uncertainty in measurement" — Propagation of distributions using a Monte Carlo method. vol. JCGM 101:2. 2008.

[7] Woodward MD. Evaluation of inter-facility uncertainty for ship manoeuvring performance prediction. Ocean Eng 2014;88:598–606. doi:10.1016/j.oceaneng.2014.04.001.

[8] Dash AK, Nagarajan V, Sha OP. Uncertainty assessment for ship maneuvering mathematical model. Int Shipbuild Prog 2015;62:57–111. doi:10.3233/ISP-150117.

[9] ISO. Evaluation of measurement data — Guide to the expression of uncertainty in measurement. Int Organ Stand Geneva ISBN 2008;50:134.

doi:10.1373/clinchem.2003.030528.

[10] Saltelli A, Annoni P, Azzini I, Campolongo F, Ratto M, Tarantola S. Variance based sensitivity analysis of model output. Design and estimator for the total sensitivity index. Comput Phys Commun 2010;181:259–70. doi:10.1016/j.cpc.2009.09.018.

[11] Saltelli A, Ratto M, Andres T, Campolongo F, Cariboni J, Gatelli D, et al. Global Sensitivity Analysis. The Primer. Chichester, UK: John Wiley & Sons, Ltd; 2007. doi:10.1002/9780470725184.

[12] IMO. Explanatory notes to the standards for ship manoeuvrability. vol. 137. 2002. doi:10.3940/rina.sbt.1998.a7.

[13] Fossen TI. Handbook of Marine Craft Hydrodynamics and Motion Control. Chichester, UK: John Wiley & Sons, Ltd; 2011. doi:10.1002/9781119994138.

[14] Khanfir S, Hasegawa K, Nagarajan V, Shouji K, Lee SK. Manoeuvring characteristics of twin-rudder systems: Rudder-hull interaction effect on the manoeuvrability of twin-rudder ships. J Mar Sci Technol 2011;16:472–90. doi:10.1007/s00773-011-0140-3.

[15] Brix JE, editor. Manoeuvring Technical Manual. Seehafen-Verlag; 1993.

[16] Molland AF, Turnock SR. Front Matter. Mar. Rudders Control Surfaces, Elsevier; 2007, p. iii. doi:10.1016/B978-0-7506-6944-3.50018-4.

Appendix. Description of simulation model

In this study, we use a relatively simple 3-degrees-of-freedom modular mathematical model. The model is mainly based on [13–15]. Figure A.1 illustrates reference systems and some corresponding notations. Coordinates of the ship $\boldsymbol{\eta} = [X\ Y\ \psi]^T$ are expressed in the inertial reference frame *{O-**X**-**Y**}*, or *{i}*. Velocities of the ship $\boldsymbol{\upsilon} = [u\ v\ r]^T$ are expressed in the reference frame that moves with the ship *{C-**x**-**y**}*, or *{b}*, with the origin at *Lpp*/2 and axes ***x*** and ***y*** pointing forward and toward starboard, respectively.

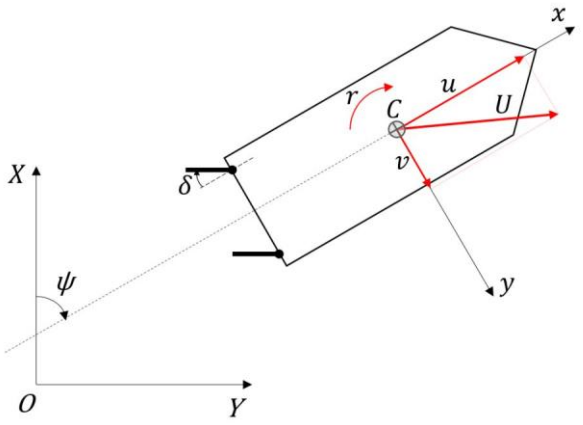

Figure A.1. Reference systems: inertial {O-**X**-**Y**} and body-fixed {C-**x**-**y**}.

The velocities in *{b}* and *{i}* are related as follows:

$$\dot{\boldsymbol{\eta}} = \boldsymbol{R}(\psi)\boldsymbol{\upsilon} \tag{A.1}$$

where $\boldsymbol{R}(\psi)$ is the rotation matrix from *{b}* to *{i}*. The manoeuvring model is expressed in *{b}* in general form as (see, for instance, [13]):

$$\begin{bmatrix} m-X_{\dot{u}} & 0 & 0 \\ 0 & m-Y_{\dot{v}} & mx_G-Y_{\dot{r}} \\ 0 & mx_G-N_{\dot{v}} & I_{zz}-N_{\dot{r}} \end{bmatrix}\begin{bmatrix} \dot{u} \\ \dot{v} \\ \dot{r} \end{bmatrix} + m\begin{bmatrix} -vr-x_G r^2 \\ ur \\ x_G ur \end{bmatrix} = \begin{bmatrix} X_H+X_P+X_R+X_W \\ Y_H+Y_R+Y_W \\ N_H+N_P+N_R+N_W \end{bmatrix} \tag{A.2}$$

The subscripts *'H', 'P', 'R'* and *'W'* refer to the hull, propeller, rudder and wind forces, respectively. In the presence of a constant irrotational current with speed V_C and direction α_C, (A.2) holds for relative velocities (see [13]), defined as

$$\begin{aligned} u_r &= u - V_C\cos(\alpha_C - \psi) \\ v_r &= v - V_C\sin(\alpha_C - \psi) \end{aligned} \tag{A.3}$$

Let us now consider the components of forces and moment on the right-hand side of (A.2). We use the following representation of the hull hydrodynamic velocity-dependent forces:

$$\begin{aligned} X_H &= X(u) - Y_{\dot{v}}vr - Y_{\dot{r}}r^2 \\ Y_H &= X_{\dot{u}}ur + Y_v v + Y_r r + Y_{v|v|}v|v| + Y_{r|v|}r|v| + Y_{v|r|}v|r| + Y_{r|r|}r|r| \\ N_H &= Y_{\dot{r}}ur + (Y_{\dot{v}} - X_{\dot{u}})uv + N_v v + N_r r + N_{v|v|}v|v| + N_{r|v|}r|v| + N_{v|r|}v|r| + N_{r|r|}r|r| \end{aligned} \tag{A.4}$$

where *X(u)* is ship resistance. The propulsion forces are calculated using a propeller open water characteristic $K_T(J)$:

$$\begin{aligned} X_P &= (1-t)\rho D_p^4 \left\{ n_1^2 K_T(J_1) + n_2^2 K_T(J_2) \right\} \\ N_P &= -(1-t)\rho D_p^4 \left\{ y_{p1} n_1^2 K_T(J_1) + y_{p2} n_2^2 K_T(J_2) \right\} \end{aligned} \tag{A.5}$$

where

$$J_i = \frac{(1-w_i)u}{n_i D_p}, \quad i = \{1,2\} \tag{A.6}$$

Here and in the following expressions, the subscripts '1' and '2' refer to the starboard and port sides, respectively. Forces acting on a rudder are based on lift and drag coefficients (see Figure A.2 for the angles definitions):

$$\begin{aligned} X_{Ri} &= \frac{1}{2}\rho V_{Ri}^2 A_R \left(-C_L \sin\vartheta_i - C_D \cos\vartheta_i \right) \\ Y_{Ri} &= \frac{1}{2}\rho V_{Ri}^2 A_R \left(C_L \cos\vartheta_i - C_D \sin\vartheta_i \right) \end{aligned} \tag{A.7}$$

where

$$V_{Ri} = \sqrt{u_{Ri}^2 + v_{Ri}^2} \tag{A.8}$$

We assume that the whole rudder is situated within the propeller slipstream. Longitudinal inflow velocity is calculated as follows:

$$u_{Ri} = J_i n_i D_p \varepsilon \left[1 + \frac{K_R}{\varepsilon} \left\{ \sqrt{1 + \frac{8K_T(J_i)}{\pi J_i^2}} - 1 \right\} \right] \tag{A.9}$$

where

$$K_R = 0.5 + \frac{0.5}{1 + 0.15/\left((x_P - x_R)/D_P \right)} \tag{A.10}$$

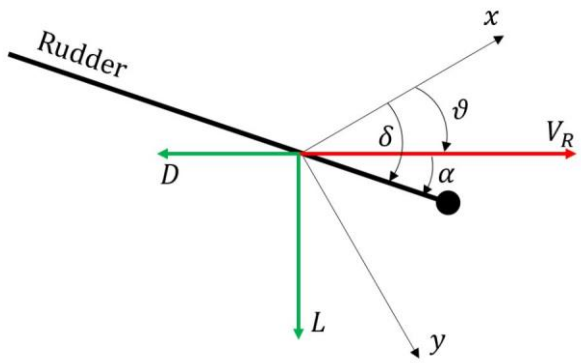

Figure A.2. Rudder inflow velocity and forces.

The inflow to the rudders is affected by flow straightening:

$$v_{Ri} = \gamma_i \left(v + r x_R \right) \tag{A.11}$$

Thus,

$$\vartheta_i = \text{atan}\left(\frac{v_{Ri}}{u_{Ri}} \right) \tag{A.12}$$

and

$$\alpha_i = \delta_i - \vartheta_i \tag{A.13}$$

The total rudder lateral force and moment include the rudders-hull interaction via the rudder-hull interaction coefficients a_H, t_R and x_H:

$$\begin{aligned} X_R &= \left(1 - t_R\right)\left(X_{R1} + X_{R2} \right) \\ Y_R &= \left(1 + a_H\right)\left(Y_{R1} + Y_{R2} \right) \\ N_R &= \left(x_R + x_H a_H \right)\left(Y_{R1} + Y_{R2} \right) \end{aligned} \tag{A.14}$$

Finally, the wind forces and moment are calculated according to [15]:

$$\begin{aligned} X_W &= \frac{1}{2} \rho_{air} V_{W,a}^2 A_F C_{W,X} \\ Y_W &= \frac{1}{2} \rho_{air} V_{W,a}^2 A_L C_{W,Y} \\ N_W &= \frac{1}{2} \rho_{air} V_{W,a}^2 A_L L C_{w,N} \end{aligned} \tag{A.15}$$

where ρ_{air} is air density, $V_{W,a}$ is the apparent speed of wind, A_F and A_L are the frontal and lateral projected areas of the ship, and L is the overall length of the ship.

The hydrodynamic coefficients of the hull in (A.4) are estimated from PMM tests. Table A.1 lists the non-dimensional coefficients (terms $\rho Lpp^2U^2/2$ and $\rho Lpp^3U^2/2$ are used as dimensional factors for forces and moment, respectively; U=5.28 m/s).

Table A.1. Hull hydrodynamic coefficients in non-dimensional form, 10^{-4}.

X_u'	-0.89	Y_r'	19.09
X_{uu}'	-0.79	$Y_{v\|v\|}'$	-19.68
X_{uuu}'	-0.90	$Y_{r\|r\|}'$	2.46
X_{uuuu}'	-1.10	$Y_{v\|r\|}'$	1.15
X_{uuuuu}'	-0.63	$Y_{r\|v\|}'$	3.34
$X_{\dot{u}}'$	-6.12	N_v'	20.55
$Y_{\dot{v}}'$	-37.34	N_r'	-6.23
$Y_{\dot{r}}'$	0.47	$N_{v\|v\|}'$	15.86
$N_{\dot{v}}'$	0.47	$N_{r\|r\|}'$	-2.19
$N_{\dot{r}}'$	-1.12	$N_{v\|r\|}'$	2.18
Y_v'	-66.05	$N_{r\|v\|}'$	-6.16

Coefficients C_L and C_D for the flapped rudder are evaluated based on the results of open water tests found in [16]. The hull-propeller-rudder interaction coefficients are estimated from the free running model tests. The wind coefficients $C_{W,X}$, $C_{W,Y}$ and $C_{W,N}$ for the research vessel are found in [15].